

High-Stretchability, Ultralow-Hysteresis Conducting Polymer Hydrogel Strain Sensors for Soft Machines

Zequan Shen, Zhilin Zhang, Ningbin Zhang, Jinhao Li, Peiwei Zhou, Faqi Hu, Yu Rong, Baoyang Lu,* and Guoying Gu*

Highly stretchable strain sensors based on conducting polymer hydrogel are rapidly emerging as a promising candidate toward diverse wearable skins and sensing devices for soft machines. However, due to the intrinsic limitations of low stretchability and large hysteresis, existing strain sensors cannot fully exploit their potential when used in wearable or robotic systems. Here, a conducting polymer hydrogel strain sensor exhibiting both ultimate strain (300%) and negligible hysteresis (<1.5%) is presented. This is achieved through a unique microphase semiseparated network design by compositing poly(3,4-ethylenedioxythiophene):polystyrene sulfonate (PEDOT:PSS) nanofibers with poly(vinyl alcohol) (PVA) and facile fabrication by combining 3D printing and successive freeze-thawing. The overall superior performances of the strain sensor including stretchability, linearity, cyclic stability, and robustness against mechanical twisting and pressing are systematically characterized. The integration and application of such strain sensor with electronic skins are further demonstrated to measure various physiological signals, identify hand gestures, enable a soft gripper for objection recognition, and remote control of an industrial robot. This work may offer both promising conducting polymer hydrogels with enhanced sensing functionalities and technical platforms toward stretchable electronic skins and intelligent robotic systems.

1. Introduction

Strain sensors made of soft and stretchable materials are essential for electronic skins^[1–5] and soft robotics.^[6–10] To facilitate interaction compliance and precise monitoring, next-generation strain sensors are expected to provide high stretchability, fast response, and excellent repeatability in unstructured environments.^[11] Based on various types of soft functional materials, many efforts have been made to develop prototypical designs of diverse strain sensors with conductive nanomaterials,^[12,13] hydrogels,^[14–19] and liquid metals.^[20,21] Among them, conducting polymer hydrogels can provide both ionic and electronic conductivity and thus rapidly emerge as the promising candidate with several specific advantages of the intrinsic stretchability, stable conductivity, biocompatibility and mechanical robustness.^[22,23] Recent studies have reported the design of soft conducting polymer hydrogel strain sensors to enable sensitive electrical response under physical strain.^[24,25] For instance,

through solution-based blending of poly(3,4-ethylenedioxythiophene):poly(styrenesulfonate) (PEDOT:PSS) with polyurethane (PU) followed by coating carbon nanotubes, Roh et al.^[26] developed a strain sensor to detect human facial expressions. However, their reported devices typically suffer from low stretchability owing to the inherent limitations of rigid conducting polymers. Despite recent advances to enhance the stretchability with the elastomeric matrix, highly stretchable conducting polymer hydrogel strain sensors suffer from the high hysteresis due to the irreversible energy dissipation of viscoelastic elastomers under cyclic stretch.^[27,28] Additionally, current strain sensors are generally susceptible to the interference of off-axial distortions such as twisting and pressing when operated under unconstrained conditions.^[29,30] These limitations significantly hinder their practical applications in soft robotic systems with a large deformation range and versatile functionalities. As a result, developing mechanically robust conducting polymer hydrogel strain sensors that can address the tradeoff between high stretchability and ultralow hysteresis has not been achieved.


Here, we present a highly stretchable and hysteresis-free strain sensor based on conducting polymer hydrogels for

Z. Shen, N. Zhang, J. Li, P. Zhou, Y. Rong, G. Gu
Robotics Institute
School of Mechanical Engineering
Shanghai Jiao Tong University
Shanghai 200240, China
E-mail: guguoying@sjtu.edu.cn

Z. Shen, N. Zhang, J. Li, P. Zhou, Y. Rong, G. Gu
State Key Laboratory of Mechanical System and Vibration
Shanghai Jiao Tong University
Shanghai 200240, China

Z. Zhang, F. Hu, B. Lu
Jiangxi Key Laboratory of Flexible Electronics
Flexible Electronics Innovation Institute
Jiangxi Science and Technology Normal University
Nanchang 330013, China
E-mail: luby@jxstnu.edu.cn

G. Gu
Meta Robotics Institute
Shanghai Jiao Tong University
Shanghai 200240, China

 The ORCID identification number(s) for the author(s) of this article can be found under <https://doi.org/10.1002/adma.202203650>.

DOI: 10.1002/adma.202203650

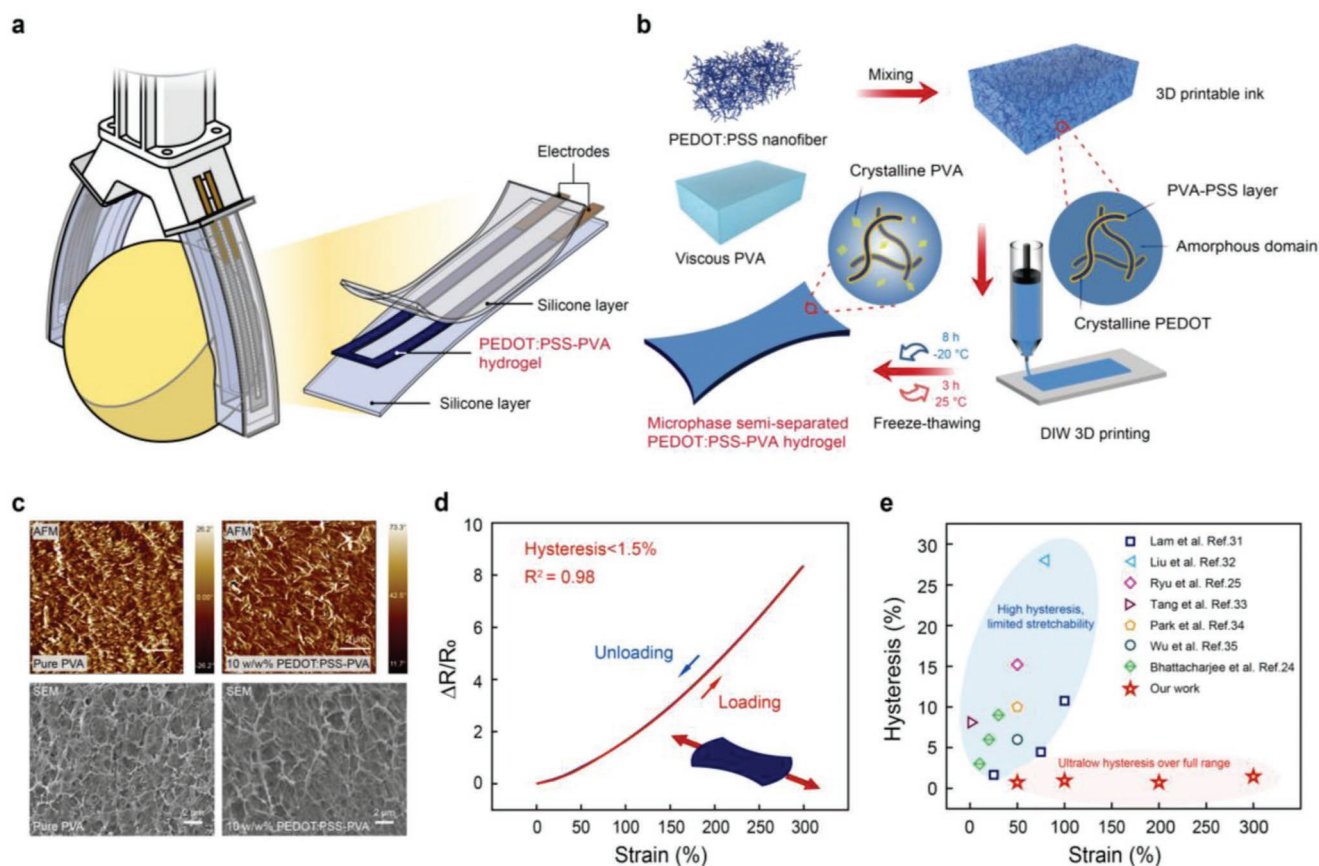


Figure 1. PEDOT:PSS-PVA hydrogel strain sensor. a) Schematic illustration of a soft robotic machine integrated with a PEDOT:PSS-PVA hydrogel strain sensor. b) Principle and fabrication process of the PEDOT:PSS-PVA conducting polymer hydrogel. c) AFM phase images (top) and SEM images (bottom) of pure PVA and 10 w/w% PEDOT:PSS-PVA hydrogel, respectively. d) Loading and unloading resistance responses of the PEDOT:PSS-PVA hydrogel strain sensor with a strain of 300%, exhibiting ultralow hysteresis ($<1.5\%$) and linearity $R^2 = 0.98$. e) Comparison of the hysteresis and strain performance of our PEDOT:PSS-PVA hydrogel strain sensor with existing PEDOT:PSS-based strain sensors.

wearable skins and soft robots (Figure 1a). A facile one-step compositing methodology is developed to create a unique microphase semiseparated network of conducting polymer hydrogels by combining PEDOT:PSS nanofibers with poly(vinyl alcohol) (PVA). We take advantage of direct-ink-writing (DIW) 3D printing and successive freeze-thawing for scalable fabrication. We next demonstrate that our PEDOT:PSS-PVA hydrogel strain sensors can simultaneously exhibit high stretchability (300%) and ultralow hysteresis ($<1.5\%$). Moreover, our strain sensors also achieve a set of other superior properties including high linearity, mechanical cyclic stability, and intrinsic robustness resistant to off-axial deformations such as torsion and pressure. To harness these enhanced sensing properties of the sensors, we demonstrate their applications as wearable skins capable of continuously monitoring physiological signals like human swallowing and blinking. We further develop a multiplex sensing patch mounted on the back of the hand to recognize gestures through detecting subtle deformations of human skins. Lastly, we demonstrate that such wearable skins can detect human motions to provide remote control signal for industrial robot movements and be integrated within a soft gripper enabling object recognition. The practical applications of our PEDOT:PSS-PVA hydrogel strain sensors indicate

the substantial potential in next-generation soft intelligent machines and robots.

2. Results

2.1. Design of the PEDOT:PSS-PVA Hydrogel Strain Sensor

Based on the resistive sensing principle,^[14] we design a class of prototypical conducting-polymer hydrogel strain sensors with a sandwiched structure, in which the PEDOT:PSS-PVA hydrogel serves as the intermediate sensing layer and silicone elastomers are covered on both sides as encapsulating layers. We propose a simple phase engineering methodology, inspired by bicontinuous phase network design,^[20] to composite PEDOT:PSS with the tough hydrogel networks of PVA, which can improve the mechanical robustness and stretchability of PEDOT:PSS without compromising the excellent electrical properties.

Our compositing method involves vigorous mechanical mixing of water-dispersed PEDOT:PSS nanofibrils and viscous PVA aqueous solution followed by physical cross-linking via freeze-thawing to afford a microphase semiseparated hydrogel network (Figure 1b). In order to achieve a well-interconnected

bicontinuous phase-separated PEDOT:PSS-PVA network, we isolate PEDOT:PSS nanofibers from commercial products and controllably re-disperse them (partially soluble) into concentrated suspensions. Vigorous mechanical mixing of concentrated PEDOT:PSS and viscous PVA solutions yield a homogeneous 3D printable paste due to the secondary doping effect of polyhydroxylates (PVA) on PEDOT:PSS chains. We characterize the rheological properties of the PEDOT:PSS-PVA inks to demonstrate the printability (Figures S1 and S2, Supporting Information). Typical shear thinning response allows the inks to be extruded through the nozzles, while shear yielding property enables the inks to maintain shapes after exiting the nozzles. After 3D printing (see Movie S1, Supporting Information), successive freeze-thawing of such paste physically crosslinks PEDOT-rich semicrystalline and PVA crystalline domains within amorphous matrix, which further interlocks the phase configuration and ensures the formation of a well-distributed stable microphase semiseparated hydrogel network. In such a PEDOT:PSS-PVA hydrogel, hydrophobic PEDOT-rich crystalline domain (as the electrical phase) can guarantee stable electrical performances for strain sensing, while hydrogen bonding-crosslinked PVA domain (as the mechanical phase) enables the mechanical stretchability and robustness. The phase boundaries between the electrical and mechanical phases are merged and interlocked by multiple intermolecular interactions among PEDOT, PSS, and PVA chains, including electrostatic interaction of PSS/PVA on PEDOT, hydrogen bonding among PVA chain, and chain entanglement among long PVA and/or PSS chains (Figure S3, Supporting Information). Such a phase configuration is beneficial to effectively minimize the hysteresis without compromising the electrical/mechanical properties by eliminating the interfacial detachment and slippage issues between electronic conductors and elastomeric matrix (generally observed for common hydrogel-based strain sensing materials).

To confirm such a hydrogel network, atomic force microscopy (AFM) phase images of freeze-dried PEDOT:PSS-PVA hydrogel show that the introduction of PEDOT:PSS nanofibrils into PVA partly interrupts the crystallinity of PVA chains, resulting in a more fibrillar phase network (Figure 1c). Scanning electron microscopy (SEM) images also show that the PEDOT:PSS-PVA hydrogel presents a well-interconnected continuous network morphology with a larger size (Figure 1c). These phase evolutions and microstructural changes verify the formation of the microphase semiseparated PEDOT:PSS-PVA hydrogel network, which is responsible for the mechanical robustness and excellent strain sensing performances. Furthermore, the tradeoff between mechanical and electrical properties of the conducting-polymer hydrogel is also influenced by the PEDOT:PSS concentration. As shown in Figure S4, Supporting Information, the fracture strain and initial resistance of PEDOT:PSS-PVA hydrogels decrease with the increase of the PEDOT:PSS concentration. We thus select 10 w/w% of PEDOT:PSS as an optimal concentration for both high stretchability and conductivity.

Owing to the excellent printability of precursor PEDOT:PSS-PVA inks, we can fabricate various PEDOT:PSS-PVA hydrogel structures in a programmable, facile, and flexible manner. The 3D printed hydrogel is sealed by silicone elastomers to avoid

dehydration.^[14] A silica-based glue is used to ensure strong bonding between the hydrogel and encapsulating layers, which improves the robustness of the hierarchically patterned structure. Then, our PEDOT:PSS-PVA hydrogel strain sensor can be easily obtained after wiring. Notably, we use the commercially available materials as the encapsulation and adhesion components, which facilitates the scalability in device dimensions and volume manufacturing.

2.2. Sensing Properties of the PEDOT:PSS-PVA Hydrogel Strain Sensor

Owing to the microphase semiseparated network of PEDOT:PSS-PVA hydrogel, our fabricated strain sensor exhibits a unique set of sensing properties. Physically cross-linked PVA domains inside the hydrogel endow our strain sensor with high stretchability exceeding 300% (Figure 1d), significantly higher than the pure PEDOT:PSS hydrogel (brittle with $\approx 40\%$ ultimate tensile strain).^[23] We characterize the relative change in resistive signal of our sensor to demonstrate its superior electrical properties under different conditions of mechanical strain. Excitingly, the corresponding loading-unloading cycle of resistance response shows almost negligible hysteresis across a wide strain range up to 300%, namely, $0.73 \pm 0.27\%$ under 50% strain, $0.95 \pm 0.43\%$ under 100% strain, $0.73 \pm 0.4\%$ under 200% strain, and $1.44 \pm 0.71\%$ under 300% strain (Data presented as mean \pm standard deviation (SD), $n = 5$). Compared to previously reported PEDOT:PSS-based strain sensors,^[24,25,31–35] our PEDOT:PSS-PVA hydrogel strain sensor displays full-scale ultralow hysteresis within a wider strain range (Figure 1e). The gauge factor (GF) of our strain sensor is calculated to be 4.07, indicating its decent sensitivity suitable for general sensing application scenarios.^[11] Excellent linearity fitting between resistance change and strain can be also observed with a high R^2 of 0.98, suggesting the ease of calibration and measurement during a specific application.

We further characterize other key electrical and mechanical properties of our PEDOT:PSS-PVA hydrogel strain sensor. In addition to high stretchability, we find that the resistive response of our strain sensor is capable of detecting ultralow deformations like $12 \mu\text{m}$ ($\approx 0.05\%$ strain) (Figure S5, Supporting Information). Such a tiny strain detection can also be successively distinguished with high resolution even under a highly stretched regime (such as 100% strain) (Figure 2a). Inheriting from the intriguing mechanical properties of PEDOT:PSS-PVA hydrogel, our strain sensor shows reliable responsive ability against applied periodic loads within varying stretched regimes (Figure 2b). Moreover, it performs excellent segment stability loaded with the step-up strains of 60% to maximum 300% and then unloaded to the initial state without obvious resistance change (Figure 2c). Long-term uniaxial stretching cycling at a high strain of 100% further reveals the outstanding robustness of the electrical signal, without observing significant degradation in both sensing performance and hysteresis upon 2000 loading-unloading cycles (Figure 2d and Figure S6, Supporting Information). Notably, the fluctuations of the resistive signals are possibly due to nonuniform deformations of the PEDOT:PSS-based electrical network and disturbances of the

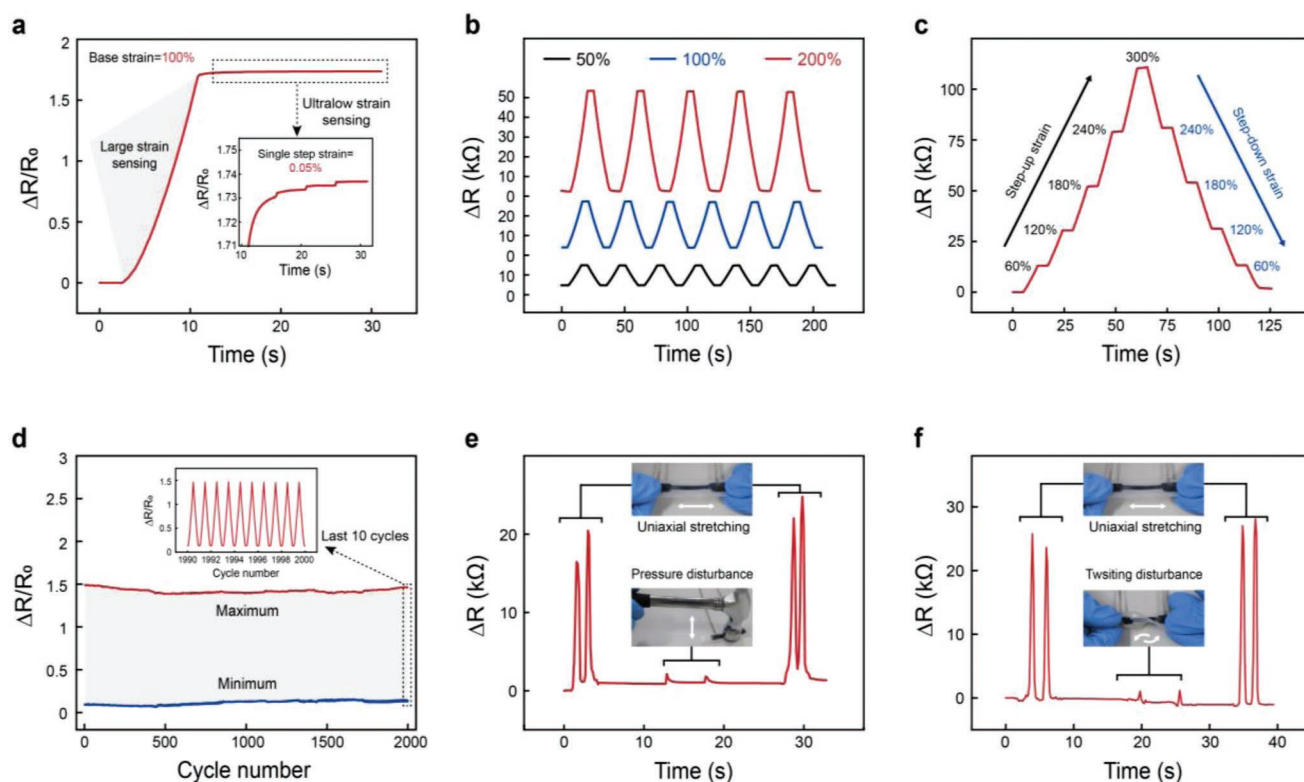


Figure 2. Sensing properties of the PEDOT:PSS-PVA hydrogel strain sensor. a) Detection of sequential single-step ultralow strains (0.05%) under a large base strain (100%). b) Resistance response of the strain sensor under periodic loading strains of 50%, 100%, and 200%, respectively. c) Resistance response of the strain sensor under a series of step-up strains of 60% to maximum 300% and next a series of step-down strains to the initial state. d) Cycling stability at a strain of 100% within 2000 cycles. The inset shows the last 10 cycles. e) Demonstration of the robustness to pressure disturbance. The insets show a sensor sample under uniaxial stretching and a hammer strike, respectively. f) Demonstration of the robustness to off-axial twisting. The insets show a sensor sample under uniaxial stretching and manually twisting, respectively.

testing motion-stage.^[18,34] Off-axial deformations like hammer strike or manual twisting (Figures 2e,f) do not cause much interference to the sensing detection, endorsing good insensitivity and decoupling deformation ability of our sensor against pressure and torsion disturbance. These superior sensing properties of our PEDOT:PSS-PVA hydrogel strain sensor readily support their potential utilization for practical applications like wearable and robotic skins.

2.3. Applications as Wearable Electronic Skins for Human Motion Detection

We use our PEDOT:PSS-PVA hydrogel strain sensors to fabricate wearable electronic skins that can monitor human motions and physiological signals. Notably, benefiting from the flexible programmability of 3D printing technique, we can facilely tailor the size and fashion of the PEDOT:PSS-PVA hydrogel strain sensors to meet varying requirements of wearable electronic skins. Additionally, desirable biocompatibility of PEDOT:PSS, PVA and commercially available silicone encapsulating layers ensure the safety of noninvasive skin contact.^[23,36,37] The experimental results show that the fabricated wearable electronic skins provide sensitive response to subtle deformations such as blinking, swallowing, and frowning (Figures 3a,b, and Figure S7, Supporting Information). From the recorded

resistance response, we can also detect the subject's blinking frequency and detailed characteristics of throat swallowing, and distinguish varying facial expressions like unsmiling, smiling and grinning (Figure 3c). More sophisticated physiological signals such as carotid artery pulse waveforms and heart rate can also be monitored by our wearable electronic skins (Figure S8, Supporting Information). For example, it can detect the real-time pulse waveforms of the subject including "P wave" (percussion), "T wave" (tidal), and "D wave" (diastolic) and successfully interpret the heart rate (94 beats min^{-1}), implying potential clinical applications of our wearable electronic skins for heart health diagnosis.^[38] Additionally, due to the ultrawide strain range, other human motions with large deformations can be easily inspected, such as elbow bending movement at 90° yielding $\approx 35\%$ strain (Figure S9, Supporting Information).

To further demonstrate the functionality for complicated sensing tasks, we design a five-pixel wearable electronic skin patch with the PEDOT:PSS-PVA hydrogel strain sensor (Figure 3d). By recording the resistance changes of all the five channels, the wearable electronic skin patch can precisely recognize hand gestures of American Sign Language from 0 to 9 after signal plotting (see Movie S2, Supporting Information), which can also be automatically classified by the machine learning approaches.^[39] The application indicates the capability of our electronic skins toward accurate recording and interpretation of complex motions.

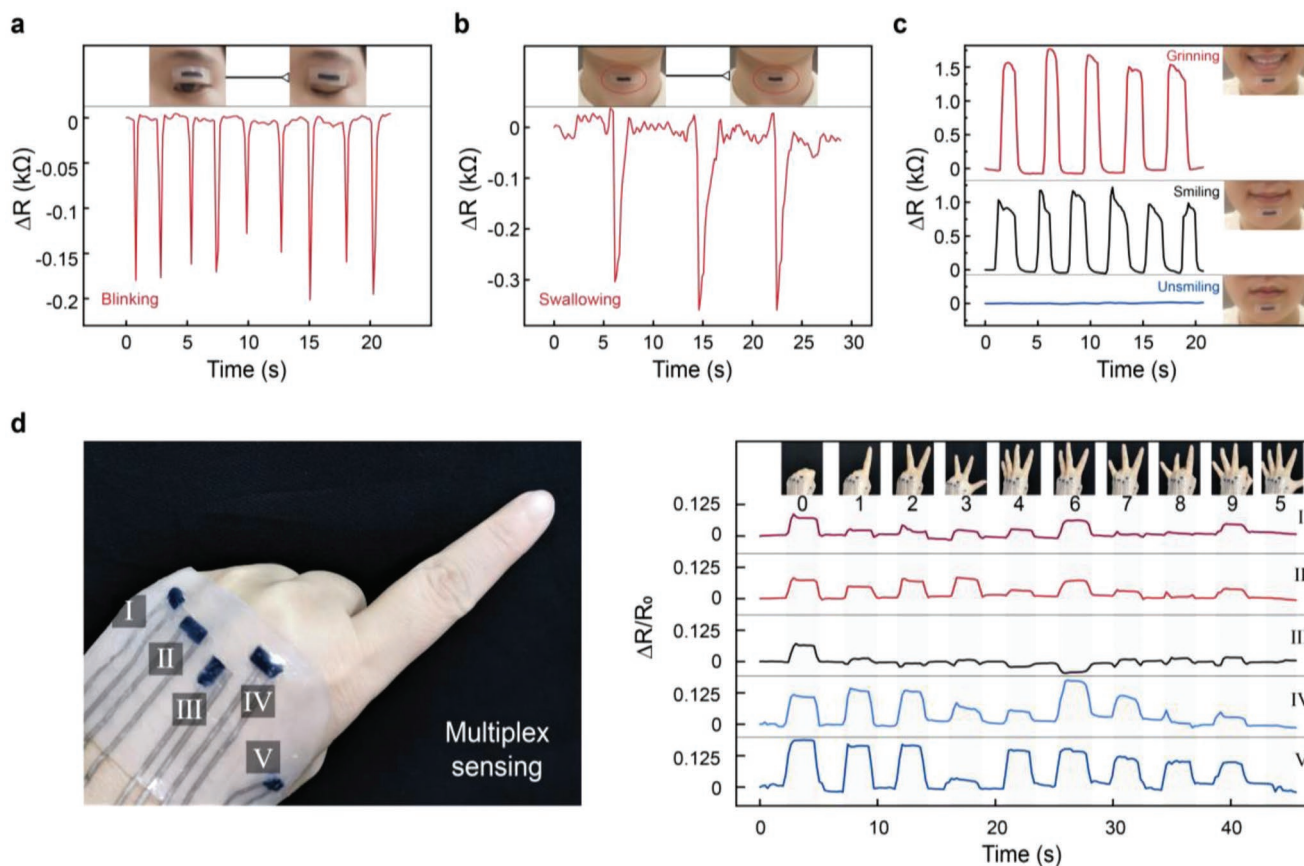


Figure 3. Wearable electronic skins for physiological monitoring and gesture recognition. a) Continuous monitoring the action of blinking. The insets show the electronic skin is attached to a subject's eyelid. b) Continuous monitoring the action of swallowing. The insets show the electronic skin is attached to a subject's throat when swallowing saliva. c) Comparison of the resistance signals when a subject is grinning, smiling and unsmiling, respectively. The insets show the electronic skin is attached to the subject's chin. d) A wearable electronic skin mounted on the back of the hand providing multiplex sensing capability for gesture recognition. Relative changes in resistance of five channels in the electronic skin when the subject performs gestures from 0 to 9. The insets show the photographs of different gestures.

2.4. Applications as Robotic Skins for Sensory Grasping and Motion Control

In view of the facile fabrication and integration, we can easily integrate our PEDOT:PSS-PVA hydrogel strain sensor into a two-finger pneumatic soft gripper to impart its sensing functionality (see the Supporting Information for the detailed fabrication process). Located inside the outer surface of the gripper, our PEDOT:PSS-PVA hydrogel strain sensor is completely immobilized and robustly integrated with the robotic skins. Due to the complexity of the surface strain of the pneumatic gripper, we harness the readily available bending angle (θ) of the actuated finger to reflect the strain. The experimental results show that the soft gripper can autonomously sense its bending angle with the stepwise increase of the pneumatic pressure from 0 to 60 kPa (Figure 4a). We further demonstrate the sensory gripper can automatically discriminate the sizes of grasping objects through the strain changes under varying pneumatic pressure actuations (Figure 4b). Further analyses show that the normalized resistance changes of the sensor linearly increase with supplied pneumatic pressure and the soft

gripper can distinguish the loading and unloading conditions based on the sensing information under the same pneumatic pressure (Figure 4c). As illustrated in Figure S10, Supporting Information, the relative changes in resistance of the robotic skin can also be linearly calibrated with the bending angles of the pneumatic gripper.

Lastly, we demonstrate that a subject can wear our PEDOT:PSS-PVA hydrogel strain sensors to remotely control an industrial robot by hand (Figure 4d). In the application, the strain sensors can continuously monitor the bending motions of the corresponding fingers. Each of the fingers is preprogrammed to control one motion direction of the industrial robot. The industrial controller instructs the motions of robot according to the automatically identified sensing signals. The experimental results demonstrate that the subject can teleoperate the industrial robot to go through a target labyrinth-like trajectory on a plane (see Movie S3, Supporting Information). We thus demonstrate that the ultralow hysteresis, stable performance, and high robustness of our PEDOT:PSS-PVA hydrogel strain sensors allow precise, reliable, and real-time control of such a robotic system through multiple sensing channels (Figure 4e).

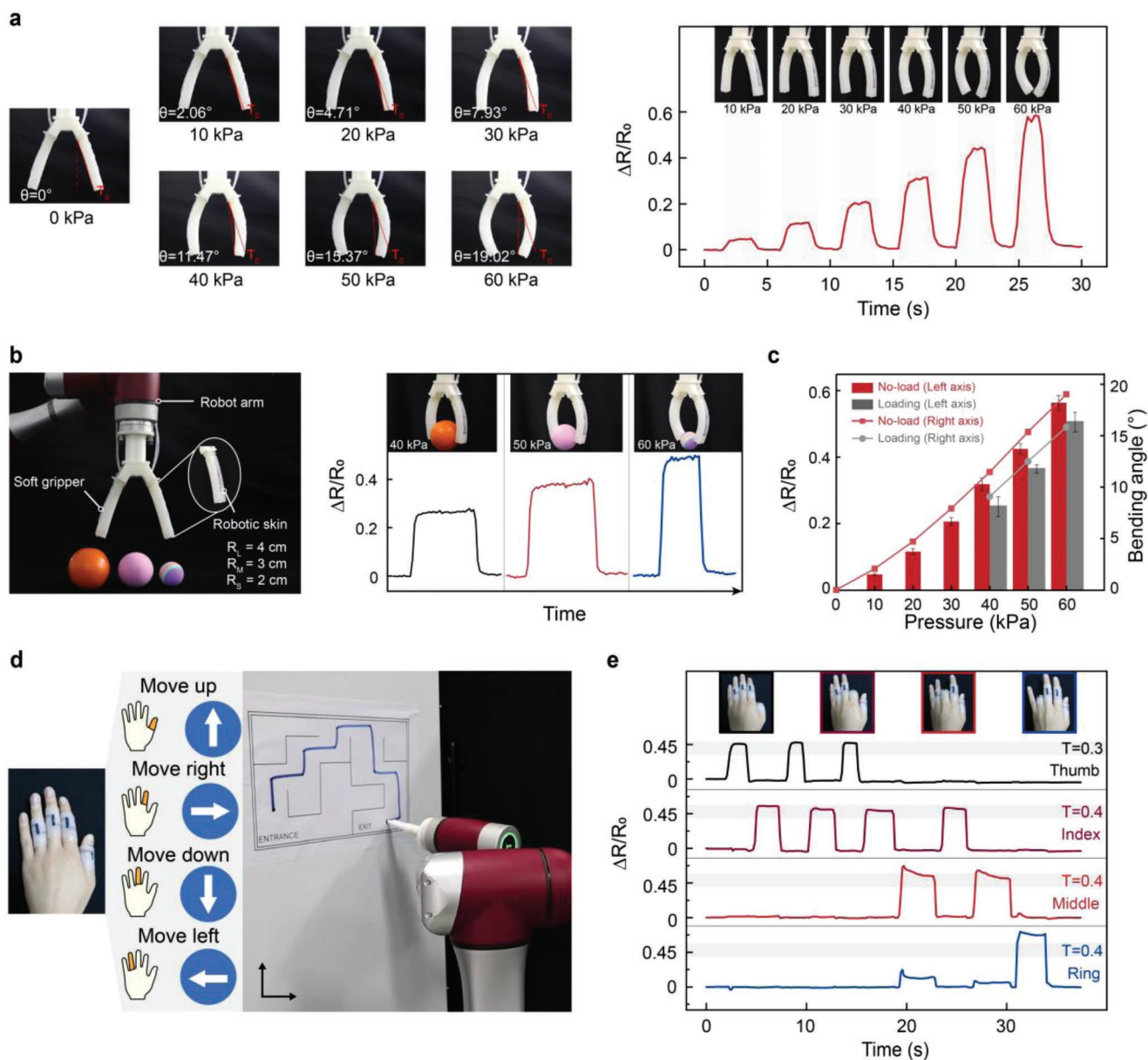


Figure 4. Robotic skins enabling sensing functionality and remote control. a) Photographs of a two-finger pneumatic soft gripper when the pressure increases from 0 to 60 kPa. The defined bending angles θ correspondingly increases from 0° to 19.02° . Relative change in resistance of the robotic skin as the pneumatic pressure gradually increases. The insets show the side-view photographs of the gripper integrated with the robotic skin under different pressure conditions. b) Photograph of the experimental setup with the sensory soft gripper mounted on an industrial robot, which is capable of grasping spherical objects with different radii. Demonstration of the capability of the sensory gripper to distinguish sizes of three spherical objects. c) Relative changes in resistance and bending angles of the sensory gripper under loading and unloading conditions, when pneumatic pressure increases from 0 to 60 kPa. Data presented as mean \pm SD, $n = 3$. d) A sensory robotic system where a subject can remotely control an industrial robot to go through a labyrinth by the wearable electronic skins. The electronic skins can detect the bending of fingers and deliver control signals instructing horizontal or vertical movements. e) Relative changes in resistance of four channels in the electronic skins during the targeted labyrinth task. The insets show the photographs of different bent fingers.

3. Conclusion

We have presented the design, fabrication and application of PEDOT:PSS-PVA hydrogel strain sensors. We further compare our strain sensors with other previously reported PEDOT-PVA based strain sensors.^[34,40–47] The result demonstrates that our sensors harness superior performances of high stretchability,

ultralow hysteresis, cyclic stability, and robustness against mechanical twisting and pressing (see Table S1, Supporting Information). This is achieved through a unique microphase semiseparated network design by compositing PEDOT:PSS nanofibers with PVA and facile fabrication by combining 3D printing and successive freeze-thawing. We also demonstrate their integration and applications as wearable electronic skins

for human-machine interaction and perception feedback for soft machines. In addition to uniaxial stretching, homogeneous sensing properties of strain sensors in different directions require further explorations. Moreover, the temperature-dependent behavior of soft strain sensors is important for long-term applications.^[29] It is often challenging because of their material nonlinearity and time-dependent viscoelastic behavior,^[48] which will be investigated in the future. The current study not only addresses a critical challenge in developing high-performance strain sensors based on conducting-polymer-hydrogels, but also offers a promising route toward next-generation intelligent robotic systems.

4. Experimental Section

Preparation of the PEDOT:PSS-PVA Conducting Polymer Hydrogel: PEDOT:PSS nanofibrils (0.382 g, Orgacon DRY, Agfa Materials) were re-dispersed with a deionized (DI) water-dimethyl sulfoxide (DMSO, Sigma-Aldrich) mixture (5 g, DI water: DMSO = 85:15 v/v) and filtered with a syringe filter (18 μm) at room temperature. 0.7 g PVA (Mw146 000–186 000, Sigma-Aldrich) was added to 9.3 g DI water and stirred at 90 $^{\circ}\text{C}$ until completely dissolved. 9 g PVA solution (7 wt%) and 1 g PEDOT:PSS solution (7 wt%) were thoroughly mixed with a syringe filter (18 μm) and then degassed by a centrifuge for 10 min to prepare the 3D printable conducting-polymer ink with 10 w/w% PEDOT:PSS. Similarly, the printed inks could be blended by other PEDOT:PSS concentrations such as 5, 20, and 50 w/w%. In this work, the PEDOT:PSS concentration of the used samples was 10 w/w% unless otherwise specified. A commercial 3D printer (Yunying Max 1.0, Beijing Yuanzhizao Technology Co. Ltd.) was then used to print the conducting-polymer ink with a nozzle (diameter, 160 μm). The height of the printed layer was 600 μm and thus the aspect ratio (height/width) was 3.75:1. The spatial resolution between two extruded strips of ink was 500 μm . Printing paths were converted to G-code by a commercial software (Tian Guang 1.1) to command the x - y - z motion of the printer head. The 3D printed PEDOT:PSS-PVA conducting-polymer sample was frozen at -20°C for 8 h and then thawed at 25 $^{\circ}\text{C}$ for 3 h. The freeze-thawed process was repeated for three times followed by swelling the dried sample in PBS solution to produce the PEDOT:PSS-PVA conducting-polymer hydrogel.

Preparation of the PEDOT:PSS-PVA Hydrogel Strain Sensor: The PEDOT:PSS-PVA hydrogel was sandwiched between two encapsulating elastomers which were made of silicone rubber (Dragon skin 00–10, Smooth-on Inc.). The Dragon skin Parts A and B were mixed (1A:1B by weight) followed by vacuum degassed for 5 min to eliminate air bubbles. The liquid rubber was plated by using an automatic film applicator (ZAA 2300, Zehntner GmbH) and then cured at 60 $^{\circ}\text{C}$ for 1 h to produce thin silicon elastomers (thickness, 300 μm). The inside of silicone elastomers was pretreated by using a type of commercial silica-based glue (Valigoo Co., Ltd.) to ensure the adhesion between the layers. Stainless steel meshes (Tianhong Co., Ltd.) were employed as electrode wires to conduct electrical signals which were attached with the conducting polymer hydrogel.

Characterization and Measurements: The degree of hysteresis (DH) was calculated by $\text{DH} = |A_L - A_U|/A_L$, where A_L and A_U were the area under loading and unloading curves given a specific strain, respectively. The GF was characterized by $\text{GF} = \delta(\Delta R/R_0)/\delta\varepsilon$, where ΔR and R_0 are the changes in resistance after applying a strain ε and the initial resistance, respectively. AFM phase images of the PEDOT:PSS-PVA hydrogel were acquired by AFM (MFP-3D, Oxford Instruments plc). SEM images of the PEDOT:PSS-PVA hydrogel were acquired by SEM (JSM-7800F, JEOL Ltd.). The rheological properties of the printed PEDOT:PSS-PVA inks were characterized by using a rotational rheometer (Discovery HR-2, TA Instruments Inc.). The applied smallest size of the strain sensor was 9 mm \times 4.5 mm and the largest size was 20 mm \times 4.5 mm. The size range had the same order of magnitude as other previously reported strain

sensors.^[49,50] The strain sensor was characterized using a computer-controlled stepping motor-driven stage (HST-200, OptoSigma Inc.). The resistance signal of the strain sensor was measured by the precise LCR (inductance–capacitance–resistance) meter (E4980AL, Keysight Technologies Inc.). Before the long-term cycling experiment, the strain sensor had been repeatedly pre-stretched and relaxed for about 300 cycles to stabilize the electrical properties. The multiplex resistance signals of the wearable electronic skins were processed by MATLAB (The MathWorks, Inc.). The soft gripper was fixed on the end of an industrial robot (Jaka Co., Ltd.). The control signals were transmitted to the industrial controller of the industrial robot through Transmission Control Protocol/Internet Protocol (TCP/IP) via MATLAB. All the above experiments of the strain sensors were conducted at room temperature about 25 $^{\circ}\text{C}$.

Statistical Analysis: Data were presented as mean values \pm standard deviation with sample size ($n = 3$ – 5) as specified in the experiments. Statistical analysis was carried out using Origin Software.

Participant Recruitments: All experiments were conducted in accordance with the declaration of Helsinki and approved by the Institutional Review Board for Human Research Protections of Shanghai Jiao Tong University. All human participants took part in the experiments voluntarily with informed consent.

Supporting Information

Supporting Information is available from the Wiley Online Library or from the author.

Acknowledgements

This study was supported in part by the National Natural Science Foundation of China (Grant Nos. 52025057, 51963011 and 91948302), the Science and Technology Commission of Shanghai Municipality (Grant No. 20550712100) and the Innovative Research Team of High-Level Local Universities in Shanghai (SHSMU-ZDCX20210901). The images of the participant in Figure 3a–c are published in this paper with their consent.

Conflict of Interest

The authors declare no conflict of interest.

Author contributions

Z.S. and Z.Z. contributed equally to this work. G.G. and B.L. conceived the idea and directed the project. Z.S. and Z.Z. designed the study. Z.S., Z.Z., N.Z., J.L., P.Z., F.H., and Y.R. conducted the experiments. Z.S., Z.Z., G.G., and B.L. analyzed and interpreted the results. All the authors contributed to the writing and editing of the paper.

Data Availability Statement

The data that support the findings of this study are available from the corresponding author upon reasonable request.

Keywords

conducting polymer hydrogels, electronic skin, robotic skins, strain sensors, wearable electronics

Received: April 23, 2022

Revised: June 5, 2022

Published online: July 11, 2022

- [1] X. Yu, Z. Xie, Y. Yu, J. Lee, A. Vazquez-Guardado, H. Luan, J. Ruban, X. Ning, A. Akhtar, D. Li, B. Ji, Y. Liu, R. Sun, J. Cao, Q. Huo, Y. Zhong, C. Lee, S. Kim, P. Gutruf, C. Zhang, Y. Xue, Q. Guo, A. Chempakasseril, P. Tian, W. Lu, J. Jeong, Y. Yu, J. Cornman, C. Tan, B. Kim, *Nature* **2019**, 575, 473.
- [2] S. Sundaram, P. Kellnhofer, Y. Li, J. Y. Zhu, A. Torralba, W. Matusik, *Nature* **2019**, 569, 698.
- [3] S. Lee, S. Franklin, F. A. Hassani, T. Yokota, M. O. G. Nayeem, Y. Wang, R. Leib, G. Cheng, D. W. Franklin, T. Someya, *Science* **2020**, 370, 966.
- [4] Y. Kim, A. Chortos, W. Xu, Y. Liu, Y. Oh Jin, D. Son, J. Kang, M. Foudeh Amir, C. Zhu, Y. Lee, S. Niu, J. Liu, R. Pfattner, Z. Bao, T.-W. Lee, *Science* **2018**, 360, 998.
- [5] F. Ershad, A. Thukral, J. Yue, P. Comeaux, Y. Lu, H. Shim, K. Sim, N. I. Kim, Z. Rao, R. Guevara, L. Contreras, F. Pan, Y. Zhang, Y. S. Guan, P. Yang, X. Wang, P. Wang, X. Wu, C. Yu, *Nat. Commun.* **2020**, 11, 3823.
- [6] T. G. Thuruthel, B. Shih, C. Laschi, M. T. Tolley, *Sci. Robot.* **2019**, 4, eaav1488.
- [7] S. Y. Kim, Y. Choo, R. A. Bilodeau, M. C. Yuen, G. Kaufman, D. S. Shah, C. O. Osuji, R. Kramer-Bottiglio, *Sci. Rob.* **2020**, 5, eaay3604.
- [8] J. W. Booth, D. Shah, J. C. Case, E. L. White, M. C. Yuen, O. Cyr-Choiniere, R. Kramer-Bottiglio, *Sci. Rob.* **2018**, 3, eaat1853.
- [9] Z. Shen, F. Chen, X. Zhu, K. T. Yong, G. Gu, *J. Mater. Chem. B* **2020**, 8, 8972.
- [10] G. Gu, N. Zhang, H. Xu, S. Lin, Y. Yu, G. Chai, L. Ge, H. Yang, Q. Shao, X. Sheng, X. Zhu, X. Zhao, *Nat. Biomed. Eng.* **2021**, <https://doi.org/10.1038/s41551-021-00767-0>.
- [11] A. Qiu, P. Li, Z. Yang, Y. Yao, I. Lee, J. Ma, *Adv. Funct. Mater.* **2019**, 29, 1806306.
- [12] Z. Cui, W. Wang, L. Guo, Z. Liu, P. Cai, Y. Cui, T. Wang, C. Wang, M. Zhu, Y. Zhou, W. Liu, Y. Zheng, G. Deng, C. Xu, X. Chen, *Adv. Mater.* **2022**, 34, 2104078.
- [13] C. Tan, Z. Dong, Y. Li, H. Zhao, X. Huang, Z. Zhou, J. W. Jiang, Y. Z. Long, P. Jiang, T. Y. Zhang, B. Sun, *Nat. Commun.* **2020**, 11, 3530.
- [14] J. Y. Sun, C. Keplinger, G. M. Whitesides, Z. Suo, *Adv. Mater.* **2014**, 26, 7608.
- [15] X. Liu, J. Liu, S. Lin, X. Zhao, *Mater. Today* **2020**, 36, 102.
- [16] Y. Ohm, C. Pan, M. J. Ford, X. Huang, J. Liao, C. Majidi, *Nat. Electron.* **2021**, 4, 313.
- [17] B. Ying, R. Z. Chen, R. Zuo, J. Li, X. Liu, *Adv. Funct. Mater.* **2021**, 31, 2104665.
- [18] C.-Z. Hang, X.-F. Zhao, S.-Y. Xi, Y.-H. Shang, K.-P. Yuan, F. Yang, Q.-G. Wang, J.-C. Wang, D. W. Zhang, H.-L. Lu, *Nano Energy* **2020**, 76, 105064.
- [19] Y. Zhang, P. He, M. Luo, X. Xu, G. Dai, J. Yang, *Nano Res.* **2020**, 13, 919.
- [20] E. J. Markvicka, M. D. Bartlett, X. Huang, C. Majidi, *Nat. Mater.* **2018**, 17, 618.
- [21] S. Liu, D. S. Shah, R. Kramer-Bottiglio, *Nat. Mater.* **2021**, 20, 851.
- [22] X. Fan, W. Nie, H. Tsai, N. Wang, H. Huang, Y. Cheng, R. Wen, L. Ma, F. Yan, Y. Xia, *Adv. Sci.* **2019**, 6, 1900813.
- [23] H. Yuk, B. Lu, S. Lin, K. Qu, J. Xu, J. Luo, X. Zhao, *Nat. Commun.* **2020**, 11, 1604.
- [24] M. Bhattacharjee, M. Soni, P. Escobedo, R. Dahiya, *Adv. Electron. Mater.* **2020**, 6, 2000445.
- [25] J. Ryu, J. Kim, J. Oh, S. Lim, J. Y. Sim, J. S. Jeon, K. No, S. Park, S. Hong, *Nano Energy* **2019**, 55, 348.
- [26] E. Roh, B.-U. Hwang, D. Kim, B.-Y. Kim, N.-E. Lee, *ACS Nano* **2015**, 9, 6252.
- [27] X. Meng, Y. Qiao, C. Do, W. Bras, C. He, Y. Ke, T. P. Russell, D. Qiu, *Adv. Mater.* **2022**, 34, 2108243.
- [28] H. Yao, W. Yang, W. Cheng, Y. J. Tan, H. H. See, S. Li, H. P. A. Ali, B. Z. H. Lim, Z. Liu, B. C. K. Tee, *Proc. Natl. Acad. Sci. U. S. A.* **2020**, 117, 25352.
- [29] O. A. Araromi, M. A. Graule, K. L. Dorsey, S. Castellanos, J. R. Foster, W. H. Hsu, A. E. Passy, J. J. Vlassak, J. C. Weaver, C. J. Walsh, R. J. Wood, *Nature* **2020**, 587, 219.
- [30] T. Kim, S. Lee, T. Hong, G. Shin, T. Kim, Y.-L. Park, *Sci. Rob.* **2020**, 5, eabc6878.
- [31] T. N. Lam, G. S. Lee, B. Kim, H. Dinh Xuan, D. Kim, S. I. Yoo, J. Yoon, *Compos. Sci. Technol.* **2021**, 210, 108811.
- [32] H. Liu, S. Zhang, Z. Li, T. J. Lu, H. Lin, Y. Zhu, S. Ahadian, S. Emaminejad, M. R. Dokmeci, F. Xu, A. Khademhosseini, *Matter* **2021**, 4, 2886.
- [33] N. Tang, C. Zhou, D. Qu, Y. Fang, Y. Zheng, W. Hu, K. Jin, W. Wu, X. Duan, H. Haick, *Small* **2020**, 16, 2001363.
- [34] H. Park, D. S. Kim, S. Y. Hong, C. Kim, J. Y. Yun, S. Y. Oh, S. W. Jin, Y. R. Jeong, G. T. Kim, J. S. Ha, *Nanoscale* **2017**, 9, 7631.
- [35] H. Wu, Q. Liu, H. Chen, G. Shi, C. Li, *Nanoscale* **2018**, 10, 17512.
- [36] S. Azadi, S. Peng, S. A. Moshizi, M. Asadnia, J. Xu, I. Park, C. H. Wang, S. Wu, *Adv. Mater. Technol.* **2020**, 5, 2000426.
- [37] J. M. Park, J. Son, H. J. An, J. H. Kim, H. G. Wu, J. I. Kim, *Phys. Med. Biol.* **2019**, 64, 105006.
- [38] W. W. Nichols, *Am. J. Hypertens.* **2005**, 18, 3S.
- [39] G. Gu, H. Xu, S. Peng, L. Li, S. Chen, T. Lu, X. Guo, *Soft Rob.* **2019**, 6, 368.
- [40] Y. Lee, H. Choi, H. Zhang, Y. Wu, D. Lee, W. S. Wong, X. S. Tang, J. Park, H. Yu, K. C. Tam, *ACS Sustainable Chem. Eng.* **2021**, 9, 17351.
- [41] Q. Rong, W. Lei, L. Chen, Y. Yin, J. Zhou, M. Liu, *Angew. Chem. Int. Ed. Engl.* **2017**, 56, 14159.
- [42] Q. Gao, M. Wang, X. Kang, C. Zhu, M. Ge, *Compos. Commun.* **2020**, 17, 134.
- [43] X. Peng, W. Wang, W. Yang, J. Chen, Q. Peng, T. Wang, D. Yang, J. Wang, H. Zhang, H. Zeng, *J. Colloid. Interface. Sci.* **2022**, 618, 111.
- [44] W. Zhao, D. Zhang, Y. Yang, C. Du, B. Zhang, *J. Mater. Chem. A* **2021**, 9, 22082.
- [45] X. Fan, N. Wang, J. Wang, B. Xu, F. Yan, *Mater. Chem. Front.* **2018**, 2, 355.
- [46] Y. Peng, M. Pi, X. Zhang, B. Yan, Y. Li, L. Shi, R. Ran, *Polymer* **2020**, 196, 122469.
- [47] A. Abed, Z. Samouh, C. Cochrane, F. Boussu, O. Cherkaoui, R. El Moznine, J. Vieillard, *Sensors* **2021**, 21, 4083.
- [48] C. Wang, K. Hu, C. Zhao, Y. Zou, Y. Liu, X. Qu, D. Jiang, Z. Li, M. R. Zhang, Z. Li, *Small* **2020**, 16, 1904758.
- [49] E. Dauzon, Y. Lin, H. Faber, E. Yengel, X. Sallenave, C. Plesse, F. Goubard, A. Amassian, T. D. Anthopoulos, *Adv. Funct. Mater.* **2020**, 30, 2001251.
- [50] F. Li, Y. Liu, X. Shi, H. Li, C. Wang, Q. Zhang, R. Ma, J. Liang, *Nano Lett.* **2020**, 20, 6176.